A New Self-Consistent Empirical Interatomic Potential Model for Oxides, Silicates, and Silica-Based Glasses

Alfonso Pedone,[†] Gianluca Malavasi,[†] M. Cristina Menziani,[†] Alastair N. Cormack,[‡] and Ulderico Segre*[,†]

Department of Chemistry and SCS Center, University of Modena and Reggio Emilia, Via G. Campi 183, 41100 Modena, Italy, and Kazuo Inamori School of Engineering, New York State College of Ceramics, Alfred University, Alfred, New York 14802

Received: February 21, 2006; In Final Form: April 20, 2006

A new empirical pairwise potential model for ionic and semi-ionic oxides has been developed. Its transferability and reliability have been demonstrated by testing the potentials toward the prediction of structural and mechanical properties of a wide range of silicates of technological and geological importance. The partial ionic charge model with a Morse function is used, and it allows the modeling of the quenching of melts, silicate glasses, and inorganic crystals at high-pressure and high-temperature conditions. The results obtained by molecular dynamics and free energy calculations are discussed in relation to the prediction of structural and mechanical properties of a series of soda lime silicate glasses.

1. Introduction

Silica-based glasses are of great importance in the fields of both technological industries and geosciences. Fiber optic waveguides, laser optics for initiating fusion reactions, and containers for radioactive waste are recent developments that demonstrate the importance, versatility, and potentiality of glass for additional uses.[1]

Insight into composition−structure−property relationships is fundamental for designing new materials of technological importance and for gaining a better understanding of geological phenomena. Computational techniques such as perfect lattice calculations,[2] lattice dynamics[3] and molecular dynamics (MD) simulations[4] are useful tools for calculating physical chemistry properties. In fact, structural properties, elastic constants, high-frequency and static dielectric constants, refractive indices, heat capacities, thermal expansion coefficients, and other thermodynamic properties can be calculated nowadays at any temperature and pressure for both glasses and crystal solids.[5−7]

As it is well-known, interatomic potentials are of fundamental importance for the accuracy of the simulated properties. Several interatomic potentials are available in the literature for SiO_2 polymorphs and vitreous silica (ν-SiO_2).[4,8−11] A Morse function was used successfully by Takada et al.[12] to study structural changes in cristobalite at high temperature and to simulate ν-SiO_2. Kieffier et al.[7,13] successfully simulated the $\alpha-\beta$ phase transition in silica cristobalite and ν-SiO_2 by means of a force field that included a Born−Huggins−Mayer two-body term, a three-body angular term, and charge−dipole and dipole−dipole interaction terms. -Goddard and co-workers[8,14] used a Morse function with configurationally dependent charges to study phase transition in silica polymorphs and ν-SiO_2. The use of variable charge potential models, in which charges are determined according to the electronegativity equalization (QEq) scheme of Rappe and Goddard,[15] proved to be a more appropriate method to study silicate structures and glasses in which the bond covalency changes with composition and instantaneous configurations. Unfortunately, MD codes in which this method has been implemented are limited by the computational effort required, and multicomponent glasses have not been studied with this method so far. Wilson et al.[16] successfully calculated the infrared spectrum for pure ν-SiO_2 by means of a potential that includes formal ionic charges and an explicit account of polarization effects.[17] Their approach was more recently applied to the simulation of bulk and surface properties of amorphous SiO_2,[18,19] but no applications to multicomponent glasses have been reported. To improve the description of the inter-tetrahedral structure of the silicon network and of the local environment surrounding modifier cations, a potential for pure silica, sodium silicate, and soda lime silicate glasses that includes polarization effects through the shell model was recently developed.[20]

A more general force field, implemented into the Cerius2 and Material Studio packages,[21] was developed for multicomponent silicate glasses by Garofalini et al.,[22] who successfully studied bulk and surface structures and diffusion processes.

However, the potentials developed by Garofalini et al.[22] were derived empirically to model structural features, and their performances in calculating mechanical properties are poor. Moreover, despite the obvious interest in the modeling of different silicates, usually the researchers develop, from time to time, the parameters that they need for the system at hand, and a general force field for these materials is still lacking in the literature.

The aim of this work is to provide a generalized self-consistent force field able to model both structures and mechanical properties of silica-based glasses with different compositions. Zachariasen[23] claimed that atomic forces in glasses and in the corresponding crystals must be of the same order of magnitude, since the observed mechanical properties are similar. In this framework, it is reasonable to assume that a force field able to reproduce properties of silicate crystals can be also successfully used to simulate silica-based glasses, as

* Author to whom correspondence should be addressed. Phone: +39 059 2055095. Fax: +39 059 373543. E-mail: segre@unimo.it.
[†] University of Modena and Reggio Emilia.
[‡] Alfred University.

10.1021/jp0611018 CCC: $33.50
Published on Web 05/28/2006

the deviation in the intermediate range order from crystal phases is mainly due to the cooling procedure applied in the simulation.

On one hand, obtaining parameters for a single crystal phase does not ensure their transferability to the other classes of silicates, but on the other hand, because of the great variety of silicate classes, to fit parameters on all of the crystals simultaneously is not feasible.

Therefore, we have derived a set of interatomic pairwise potentials for binary oxides, which are subsequently transferred to the silicate systems. Potentials developed to study oxides are available in the literature[24,25] and have been widely used in combination with the well-known Vessal's potentials[26] to model structural features in multicomponent glasses.[27−32] However, all these potentials were derived from fitting the calculated structure and properties at $T = 0$ K to experimental data at 300 K.

To produce a coherent set of potential functions, we have performed empirical fitting to structural and, when available, mechanical properties of a large set of oxides. Thermal quasi-harmonically and zero-point motion effects have been included by means of free energy minimization,[33] which is available within the GULP package.[34−37] The performance of this potential set has been tested in the prediction of structural and mechanical properties of a wide range of silicate crystals and of series of sodium silica glasses. Moreover, the reliability of the force field in modeling alumino-phosphate has been ascertained by comparing the computed structural and mechanical properties of $AlPO_4$ berlinite with those calculated with other potential models.[38,39]

2. Methodology

2.1. Interatomic Potential Derivation. The empirical fitting method implemented in the GULP package[34−37] has been used to derive the interatomic potential parameters. In this method, the parameters are derived to reproduce the experimental crystal structures (lattice parameters and atomic positions for one or more configurations) and/or crystal properties that contain information concerning the shape of the energy surface, such as elastic constants, high-frequency and static dielectric constants, lattice energy, piezoelectric constants, or phonon frequencies.

The conventional fitting procedure consists of the following steps:

(1) The structural crystal properties and the initial guess for the potential parameters are read.

(2) The six cell strains ($\epsilon(i)$, $i = 1, ..., 6$), internal strains ($\epsilon(i,j)$, $i = 1, ..., N$, $j = x, y, z$), and properties ($C_{obs}(l)$, $l = 1, ..., M$) of the initial structures are calculated with the guess potentials.

(3) The weighted sum of squares is calculated according to

$$F = \sum_{i=1}^{6} \omega_{1i}\epsilon(i)^2 + \sum_{i=1}^{N}\sum_{j=1}^{3} \omega_{2ij}\epsilon(i,j)^2 + \sum_{l=1}^{M} \omega_{3l}(C_{calc}(i) - C_{obs}(i))^2 \quad (1)$$

where ω_{1i}, ω_{2ij}, and ω_{3l} are the weighting factors that control the contribution of each term to F. The choice of the weighting factor value for each observable depends on the reliability and the precision of the experimental methods used for its determination.

(4) The value of F is minimized by varying the potential parameters. The procedure stops when the energy gradients for all atoms (i.e., the forces acting on them) are below a definite value.

It may happen that the minimization of forces sometimes leads to a worse structure. This can occur because in a harmonic approximation the displacements in the structure are given by the gradient vector multiplied by the inverse of the Hessian matrix. Hence, if the gradients get smaller but the inverse Hessian gets larger, then the displacements may get worse. Gale solved the problem by introducing the so-called relaxed fitting.[35] The main criterion used to estimate the accuracy of the potential model in the relaxed fitting method is given by the displacements of the computed structure away from the experimental configuration instead of the forces values at the experimental geometry. This means that the structure is optimized at every step in the fit and the displacements of the structural parameters are calculated instead of the energy gradients. Assuming that the local energy surface is quadratic, the displacement vector Δ is given by

$$\Delta = -\mathbf{H}^{-1}\cdot\mathbf{g} \quad (2)$$

where $\mathbf{H}$ is the Hessian matrix and $\mathbf{g}$ is the gradient vector.

In many cases, the potentials reported in the literature were derived by fitting calculated structures and properties at $T = 0$ K to experimental data obtained at 300 K. A more rigorous treatment requires that in the fitting method each observable is calculated at the temperature corresponding to the empirical data being employed. This implies that properties and crystal structures must be calculated by considering thermal forces. In fact, the temperature is explicitly included in the GULP code by means of the free energy minimization method.[33] In this work we have used the latter method, at finite temperature and pressure, in conjunction with relaxed fitting. Details on Gibbs free energy minimization can be found elsewhere.[40]

The elastic constants, at specific temperature and pressure, are defined as the second derivative of the Gibbs free energy with respect to the strain components[41]

$$C_{ij} = \frac{1}{V}\left(\frac{\partial^2 G}{\partial\epsilon_i\epsilon_j}\right)_X \quad (3)$$

This can be calculated at constant temperature (isothermal $X = T$) or at constant entropy (adiabatic $X = S$).

2.2. Potential Model. In the recent years, pairwise potentials with partial charges have been extensively used. When partial charges are assigned to ions, as in the Beest−Kramer−Santen (BKS) model, the contribution of the dispersion term in the Buckingham function becomes important and the Buckingham potential assumes unphysical values at low internuclear distances.

This can be problematic when the temperature used in the simulation is high. Therefore, many authors add a repulsive term of the type D/r^n to model the quenching of melts and glass formation.[30,42,43]

Three terms contributed to the potential used in this work: (a) long-range Coulomb potential, (b) short-range Morse function, and (c) repulsive contribution C/r^{12}, necessary to model the interaction at high temperature and pressure. Therefore, the expression for the resulting potential is given by

$$U(r) = \frac{z_i z_j e^2}{r} + D_{ij}[\{1 - e^{-a_{ij}\cdot(r-r_0)}\}^2 - 1] + \frac{C_{ij}}{r^{12}} \quad (4)$$

The Morse function is usually used in modeling bonded interactions in covalent systems (e.g., the hydroxide ion in ionic systems) in which the Coulomb term is subtracted. In this case

the physical meaning of the different quantities is well defined: D_{ij} is the bond dissociation energy, a_{ij} is a function of the slope of the potential energy well, and r_0 is the equilibrium bond distance. This is not the case here because the Coulomb term is explicitly included, and D_{ij}, a_{ij}, and r_0 should be simply considered as parameters.

A rigid ionic model with partial charges is used to handle the partial covalency of silicate systems. Given the success of the BKS potential,[6] the charge on the oxygen atom has been kept fixed at $q_O = -1.2e$. The partial charges on the cations are referred to the value of the oxygen charge for self-consistency of the force field. So, the silicon atom has a charge of $2q_O$, the alkaline ions of $0.5q_O$, and so on. It should be stressed again that these are "effective charges" and they must be treated as parameters in the potential model, and together with the short-range terms they form an "effective potential", although the physical significance of the individual terms may in some cases be uncertain.

The choice of the rigid ionic model is due to the aim of modeling the quenching of melts and structures and mechanical properties of glasses. In fact, a core−shell model should provide more accurate results for dielectric properties, surfaces, and defective crystals, but it requires a short time step in MD simulations, leading to cooling procedures for the quenching of melts that are computationally more expensive.

In this framework, the parameters for the functional form chosen have been derived from the binary oxide following the steps:

(a) The Si−O and O−O interactions have been conventionally fitted using the structural properties and the elastic tensor of α-quartz with the aim to obtain the initial guess parameters.

(b) The parameters obtained in the previous step have been refitted using relaxed fitting in conjunction with free energy minimization to take into account the effects of temperature and pressure ($T = 300$ K and $P = 1$ atm). The weighting factors have been increased to 10^4, 10^5, and 10 for lattice vectors, atom positions, and elastic constants, respectively.

(c) The cation−oxygen short-range interactions have been fitted for the binary oxides following points a and b, while the O−O interaction derived previously has been kept fixed. The Al−O parameters have been derived from the structural properties and elastic constants of α-corundum, the Mg−O ones from the MgO periclase observables, and so on.

(d) No elastic properties are available in the literature for alkaline oxides, and therefore, the number of parameters is greater than the number of observables, and a different parametrization is necessary. In these cases, the M−O parameters, with M = Li, Na, K, have been obtained by fitting the potential to silicates with the formula $M_2Si_2O_5$, with the Si−O interaction derived in point b fixed.

The Coulomb term in eq 4 is accurately evaluated through the Ewald summation.[44] In this work, the short-range potential cutoff has been set to 15 Å, the Newton−Raphson method[45] has been employed for minimization, and the approach of Fletcher and Powell[46] has been used to update the Hessian matrix.

2.3. Computation of Elastic Constants. The Gibbs free energy of each configuration has been minimized at room temperature and pressure, and the elastic compliance matrix has been calculated by the second derivative method of eq 3. Once the stiffness or elastic matrix **C** is obtained, several related mechanical properties of anisotropic materials can be derived from their matrix elements or from the matrix elements of the compliance matrix **S**

$$\mathbf{S} = \mathbf{C}^{-1} \tag{5}$$

In particular, the bulk modulus is calculated from the compliance matrix as follows

$$B^{-1} = S(1,1) + S(2,2) + S(3,3) + 2[S(3,1) + S(2,1) + S(3,2)] \tag{6}$$

and the values of the Young's modulus along three orthogonal directions are given by

$$E_k^{-1} = S(k,k) \quad k = 1, 3 \tag{7}$$

The number of independent elastic parameters depends on the symmetry of the crystalline material.[41] For isotropic materials the three principal values E_k must be equal. Moreover, the Poisson ratio ν and the shear modulus G are related to B and E by the equations

$$B = \frac{E}{3(1-2\nu)} \tag{8}$$

$$G = \frac{E}{2(1+\nu)} \tag{9}$$

so that only two elastic constants are independent.

Elastic properties for glasses can be calculated and compared with experimental data[47,48] and with those calculated using different empirical methods.[49]

TABLE 1: Molar Composition, Number of Atoms, Cell Sizes, and Densities of the xNa$_2$O−(100 − x)SiO$_2$ Simulated Glasses[a]

formulation	x Na$_2$O	number of atoms in the simulation box			density (g/cm^3)	cell size (Å)
		Na	Si	O		
SiO$_2$	0	0	512	1024	2.200	28.5290
NS10	10	102	461	973	2.294	28.1633
NS15	15	154	435	947	2.340	27.9924
NS20	20	204	410	922	2.385	27.8294
NS25	25	256	384	896	2.428	27.6788
NS30	30	308	358	870	2.469	27.5393

[a] The total number of atoms in each box is 1536.

2.4. MD Simulation of Sodium Silica Glasses. The model potentials derived have been applied to the simulation of a series of sodium silica glasses. The xNa$_2$O−(100 − x)SiO$_2$ series of glasses with $x = 0$, 10, 15, 20, 25, and 30, which will be denoted as SiO$_2$, NS10, NS15, NS20, NS25, and NS30, respectively, have been considered. Densities at room temperature have been calculated with Appen's empirical method[47] to be 2.200, 2.294, 2.340, 2.385, 2.428, and 2.469 g/cm^3, respectively.

The glass structures have been modeled by Molecular Dynamics (MD) simulation by means of the DL_POLY package.[50] For each composition 1536 atoms have been placed in a cubic box with an edge length ranging from 27.41 to 28.53 Å (Table 1), and three simulations have been performed with different starting randomly generated configurations. Integration of the equation of motion has been performed using the Verlet Leapfrog algorithm with a time step of 2 fs. To minimize the computational effort without altering the accuracy of the calculations the short-range interaction cutoff has been set to 5.5 Å. The same cooling procedure successfully used in recent works[30,43] has been used. The systems have been cooled

uniformly from 5000 to 300 K, by decreasing the temperature with steps of 500 K. The total cooling time is 470 ps with 235 $\times 10^3$ time steps and a nominal cooling rate of 1×10^{13} K/s. At each temperature a 20 000 time step relaxation has been allowed. During the first set of 6000 time steps, the velocity is scaled every time step. During the second set of 6000 time steps, velocity scaling every 40 time steps has been performed, and finally, during the last 8000 time steps, no velocity scaling was applied. The canonical ensemble NVT (Evans thermostat[51]) has been used. Data collections have been performed every 50 time steps during the last 15 000 of 35000 time steps using the microcanonical ensemble NVE.

Each glass structure obtained by the MD simulation has been analyzed in terms of radial distribution functions, bond angle distribution function, and ring size distributions using an algorithm developed by Yuan and Cormack.[52] The short-range order has been compared with the results of neutron diffraction[53−55] and extended X-ray absorption fine structure (EXAFS) studies.[56−58]

Mechanical properties (E, G, B, ν) have also been calculated for each final configuration by means of the GULP code.[36] Space group $P1$ has been used to simulate a cubic cell with no symmetry. As a consequence, non-isotropic results, with slightly different values according to the direction chosen, have been obtained. However, since the differences are small, the Young's modulus for the glass has been calculated as the average of the three principal values.

3. Results and Discussion

3.1. Binary Oxides. The potential parameters of the Morse form of eq 4 are listed in Table 2; all potentials have been derived using the relaxed fitting combined with Gibbs free energy minimization at $T = 300$ K and $P = 1$ atm, as outlined above. Structural parameters for the oxides have been obtained from the Inorganic Crystal Structure Database,[59] while the elastic constants have been obtained from ref 47. Table 3 lists the conventional cell structural parameters that are calculated with the newly derived potentials for binary oxides. Typical estimated errors of the computed structural parameters (lattice vectors, cation−oxygen distances, and cell volume) are well below 1%. Higher errors have been encountered in the elastic constant calculations; however, in this case, typical errors of 10−15% may be considered good results. In fact, experimental elastic constant measurements strictly depend on the history and the number of defects of the sample under investigation, and measures carried out in different laboratories show significant different values. As an example, we mention the case of zircon Zr_2SiO_4 in which C_{11} and C_{12} elastic constants reported in ref 60 are 423.7 and 70.3 GPa, while the values from ref 61 are 258.5 and 179.1 GPa, respectively. It is noteworthy that the overall agreement is as good as can be expected for rocksalt structured oxides because of the validity of the Cauchy relation[62] ($C_{12} = C_{44}$) since central force potentials are used.

3.2. Silicate Crystals. The potentials developed have been applied to the prediction of structures and mechanical properties of a range of silicate minerals by means of the free energy minimization technique at $T = 300$ K and $P = 1$ atm.

The results obtained are discussed in the following for structural subclasses: nesosilicates (single tetrahedrons), sorosilicates (double tetrahedrons), inosilicates (single and double chains), cyclosilicates (rings), phyllosilicates (sheets), and tectosilicates (frameworks).

The experimental structures have been used as initial models, then the free energy has been minimized, and the final structures and the elastic constants have been compared with the experimental ones available in the literature.[63]

TABLE 2: Potential Parameters of Eq 4 Derived from Binary Oxides[a]

	D_{ij} (eV)	a_{ij} (Å^{-2})	r_0 (Å)	C_{ij} (eV Å^{12})
$Li^{0.6}-O^{-1.2}$	0.001114	3.429506	2.681360	1.0
$Na^{0.6}-O^{-1.2}$	0.023363	1.763867	3.006315	5.0
$K^{0.6}-O^{-1.2}$	0.011612	2.062605	3.305308	5.0
$Be^{1.2}-O^{-1.2}$	0.239919	2.527420	1.815405	1.0
$Mg^{1.2}-O^{-1.2}$	0.038908	2.281000	2.586153	5.0
$Ca^{1.2}-O^{-1.2}$	0.030211	2.241334	2.923245	5.0
$Sr^{1.2}-O^{-1.2}$	0.019623	1.886000	3.328330	3.0
$Ba^{1.2}-O^{-1.2}$	0.065011	1.547596	3.393410	5.0
$Sc^{1.8}-O^{-1.2}$	0.000333	3.144445	3.200000	2.6
$Ti^{2.4}-O^{-1.2}$	0.024235	2.254703	2.708943	1.0
$Zr^{2.4}-O^{-1.2}$	0.206237	2.479675	2.436997	1.0
$Cr^{1.8}-O^{-1.2}$	0.399561	1.785079	2.340810	1.0
$Mn^{1.2}-O^{-1.2}$	0.029658	1.997543	2.852075	3.0
$Fe^{1.2}-O^{-1.2}$	0.078171	1.822638	2.658163	2.0
$Fe^{1.8}-O^{-1.2}$	0.418981	1.620376	2.382183	2.0
$Co^{1.2}-O^{-1.2}$	0.012958	2.361272	2.756282	3.0
$Ni^{1.2}-O^{-1.2}$	0.029356	2.679137	2.500754	3.0
$Cu^{0.6}-O^{-1.2}$	0.090720	3.802168	2.055405	1.0
$Ag^{0.6}-O^{-1.2}$	0.088423	3.439162	2.265956	1.0
$Zn^{1.2}-O^{-1.2}$	0.001221	3.150679	2.851850	1.0
$Al^{1.8}-O^{-1.2}$	0.361581	1.900442	2.164818	0.9
$Si^{2.4}-O^{-1.2}$	0.340554	2.006700	2.100000	1.0
$Ge^{2.4}-O^{-1.2}$	0.158118	2.294230	2.261313	5.0
$Sn^{2.4}-O^{-1.2}$	0.079400	2.156770	2.633076	3.0
$P^{3.0}-O^{-1.2}$	0.831326	2.585833	1.800790	1.0
$Nd^{1.8}-O^{-1.2}$	0.014580	1.825100	3.398717	3.0
$Gd^{1.8}-O^{-1.2}$	0.000132	2.013000	4.351589	3.0
$Er^{1.8}-O^{-1.2}$	0.040448	2.294078	2.837722	3.0
$O^{-1.2}-O^{-1.2}$	0.042395	1.379316	3.618701	22.0[b]

[a] Li−O, Na−O, and K−O interatomic potential parameters were derived from silicates of the formula $M_2Si_2O_5$. The cutoff of the short-range interactions was set to 15 Å (see text for details). [b] The term D/r^{12} is needed only in MD simulations and in free energy calculation at high temperature and pressure. In fact, the D_{OO} term can range between 22 and 100 eV Å^{12} without altering the results of free energy minimization at room temperature.

The structures investigated are listed in Tables 4−11, where they have been classified according to the nature of the silicate subclasses.

3.2.1. Nesosilicates. This subclass includes all silicates where the [SiO_4] tetrahedrons are isolated. Several types of silicate minerals are considered here, namely, the olivine, garnet, phenacite, zircon, and sillimanite and andalusite groups.

3.2.1.1. Olivine. The olivine structure of general formula M_2SiO_4 is based on a hexagonally close-packed oxygen sublattice with an orthorhombic unit cell. The structure has six sites: three for the oxygen, one tetrahedral site for the silicon, and two octahedral sites occupied by divalent cations. We have considered six compounds, namely, Mg_2SiO_4 (forsterite), Fe_2SiO_4 (fayalite), Mn_2SiO_4 (tephoroite), $CaMgSiO_4$ (monticellite), Ni_2SiO_4, and Co_2SiO_4. After free energy minimization at ambient conditions, the lattice vectors are reproduced with a typical error <2%, and the major errors have to be attributed to the average Si−O distance, which is about 2% smaller than the experimental one. This is due to the fact that the Si−O interaction has been fitted on α-quartz, which is a tectosilicate containing only bridging oxygen atoms. To overcome this problem one could assign, when modeling crystal structures, different short-range interactions to nonbridging oxygen (NBO) and bridging oxygen (BO), which are located at different positions in the unit cell. However, in melt materials the oxygen is able to diffuse in the bulk, and it can easily change its status from NBO to BO or vice versa. It would be necessary, therefore, to use a charge-

TABLE 3: Structural Parameters for Fitted Binary Oxides

		lattice parameters								elastic constants (10^{10} Pa)										
oxide		a (Å)	b (Å)	c (Å)	α (deg)	β (deg)	γ (deg)	V_{cell} (Å^3)	<M−O>	C_{11}	C_{22}	C_{33}	C_{44}	C_{55}	C_{66}	C_{12}	C_{13}	C_{14}	C_{23}	B
Cu_2O	expt	4.2696	4.2696	4.2696	90	90	90	77.833	1.8488	11.60			1.10			10.50				11.20
cuprite	calcd	4.2704	4.2704	4.2704	90	90	90	77.875	1.8491	10.58			1.94			11.38				11.12
	% error	0.02	0.02	0.02	0	0	0	0.05	0.02	−8.80			79			8.38				−0.71
Ag_2O	expt	4.7200	4.7200	4.7200	90	90	90	105.154	2.0438											
	calcd	4.7200	4.7200	4.7200	90	90	90	105.154	2.0438											
	% error	0.00	0.00	0.00	0	0	0	0.00	0.00											
BeO	expt	2.6750	2.6750	4.3410	90	90	120	26.901	1.6347	47.0		49.4	15.30			16.8	11.9			25.1
bromellite	calcd	2.6984	2.6984	4.3349	90	90	120	27.336	1.6439	47.58		48.1	14.39			17.87	14.39			26.27
	% error	0.87	0.87	−0.14	0	0	0	1.62	0.56	1.2		−2.6	−5.9			6.4	20.9			1.62
ZnO	expt	3.2494	3.2494	5.2038	90	90	120	47.584	1.9775	20.90		21.80	4.41			12.00	10.4			14.35
zincite	calcd	3.2463	3.2463	5.0974	90	90	120	46.522	1.9637	21.29		17.77	4.31			13.99	12.1			14.90
	% error	−0.1	−0.1	−2.0	0	0	0	−2.2	−0.7	1.87		−18.5	−2.2			16.6	16.3			3.8
MgO	expt	4.2170	4.2170	4.2170	90	90	90	74.991	2.1086	29.40			15.5			9.30				16.0
periclase	calcd	4.2394	4.2394	4.2394	90	90	90	76.192	2.1197	29.46			10.53			10.53				16.84
	% error	0.53	0.53	0.53	0	0	0	1.60	0.53	0.20			−32			13				5.3
CaO	expt	4.8105	4.8105	4.8105	90	90	90	111.319	2.4052	22.40			8.06			6.00				11.47
lime	calcd	4.7748	4.7748	4.7748	90	90	90	108.861	2.3874	26.87			4.56			4.56				11.96
	% error	−0.74	−0.74	−0.74	0	0	0	−2.2	−0.74	20			43			24				4.27
SrO	expt	5.1500	5.1500	5.1500	90	90	90	136.591	2.5750	17.00			5.56			4.6				8.73
	calcd	5.1453	5.1453	5.1453	90	90	90	136.213	2.5726	17.13			2.84			2.84				7.60
	% error	−0.09	−0.09	−0.09	0	0	0	−0.28	−0.09	0.76			−49			−38				−12.9
BaO	expt	5.5300	5.5300	5.5300	90	90	90	169.112	2.765	12.2			3.44			4.5				7.07
	calcd	5.5011	5.5011	5.5011	90	90	90	166.475	2.7505	13.78			1.71			1.71				5.73
	% error	−0.52	−0.52	−0.52	0	0	0	−1.56	−0.52	13.0			−50			−62				−19
FeO	expt	4.3000	4.3000	4.3000	90	90	90	79.507	2.1500	35.9			5.6			15.6				22.37
wustite	calcd	4.2835	4.2835	4.2835	90	90	90	78.595	2.1417	32.45			9.77			9.77				17.33
	% error	−0.38	−0.38	−0.38	0	0	0	−1.15	−0.39	−9.6			74			−37				−22.5
CoO	expt	4.2500	4.2500	4.2500	90	90	90	76.766	2.1250	26.00			8.24			14.5				18.33
	calcd	4.2425	4.2425	4.2425	90	90	90	76.361	2.1213	26.13			10.69			10.69				15.84
	% error	−0.18	−0.18	−0.18	0	0	0	−0.53	−0.17	0.5			30			−26				−13.6
NiO	expt	4.1946	4.1946	4.1946	90	90	90	73.803	2.0973	34.46			4.0			14.1				20.5
bunsenite	calcd	4.1890	4.1890	4.1890	90	90	90	73.507	2.0945	34.57			11.69			11.69				19.32
	% error	−0.13	−0.13	−0.13	0	0	0	−0.4	−0.13	0.32			192			−17				−5.8
MnO	expt	4.4448	4.4448	4.4448	90	90	90	87.813	2.2224	22.70			7.80			11.60				15.30
manganosite	calcd	4.4398	4.4398	4.4398	90	90	90	87.516	2.2199	23.66			7.48			7.48				12.87
	% error	−0.11	−0.11	−0.11	0	0	0	−0.34	−0.11	4.23			−4.1			−36				−15.9
Al_2O_3	expt	4.7602	4.7602	12.9933	90	90	120	254.977	1.9134	49.70		50.10	14.68			16.20	11.60		−2.14	25.35
α-corundum	calcd	4.7113	4.7113	13.0119	90	90	120	250.121	1.9072	48.82		50.18	11.38			19.70	15.00		−2.96	27.45
	% error	−1.03	−1.03	0.14	0	0	0	−1.9	−0.32	−1.77		0.16	−22.5			21.6	29.3		38.3	8.3
Fe_2O_3	expt	4.9666	4.9666	13.4251	90	90	120	286.792	2.0045											20.66
hematite	calcd	4.9524	4.9524	13.4237	90	90	120	285.121	1.9903											22.91
	% error	−0.29	−0.29	−0.01	0	0	0	−0.58	−0.71											10.9
Cr_2O_3	expt	4.9607	4.9607	13.5990	90	90	120	289.817	1.9906	37.40		36.2	15.9			14.80	17.50			23.40
eskolaite	calcd	5.0017	5.0017	13.5945	90	90	120	294.529	2.0086	39.32		35.31	12.82			16.89	17.5			23.73
	% error	0.83	0.83	−0.03	0	0	0	1.63	0.90	5.13		−2.5	−19.4			14.1	16.6			1.41
Sc_2O_3	expt	9.8459	9.8459	9.8459	90	90	90	954.479	2.1304											
	calcd	9.8648	9.8648	9.8648	90	90	90	959.976	2.1249											
	% error	0.19	0.19	0.19	0	0	0	0.58	−0.26											

TABLE 3: (Continued)

		lattice parameters								elastic constants (10^{10} Pa)										
oxide		*a* (Å)	*b* (Å)	*c* (Å)	α (deg)	*β* (deg)	*γ* (deg)	V_{cell} (Å^3)	<M−O>	C_{11}	C_{22}	C_{33}	C_{44}	C_{55}	C_{66}	C_{12}	C_{13}	C_{14}	C_{23}	*B*
Nd_2O_3	expt	11.0740	11.0740	11.0740	90	90	90	1358.04	2.3830											
	calcd	11.0693	11.0693	11.0693	90	90	90	1356.32	2.3847											
	% error	−0.04	−0.04	−0.04	0	0	0	−0.12	0.07											
Gd_2O_3	expt	10.8090	10.8090	10.8090	90	90	90	1262.86	2.3264											11.58
	calcd	10.8047	10.8047	10.8047	90	90	90	1261.36	2.3282											10.07
	% error	−0.04	−0.04	−0.04	0	0	0	−0.11	0.08											−13.0
Er_2O_3	expt	10.5360	10.5360	10.5360	90	90	90	1169.57	2.2711											14.04
	calcd	10.5306	10.5306	10.5306	90	90	90	1167.79	2.2677											14.43
	% error	−0.05	−0.05	−0.05	0	0	0	−0.15	−0.15											2.78
SiO_2	expt	4.9160	4.9160	5.4054	90	90	120	113.13	1.609	8.66		10.61	5.78			0.67	1.26	−1.78		3.78
α-quartz	calcd	4.9241	4.9241	5.4333	90	90	120	114.092	1.602	8.68		10.63	4.95			0.88	1.18	−1.78		3.79
	% error	0.16	0.16	0.52	0	0	0	0.85	−0.44	0.23		0.19	−14.4			31.3	−6.4	0.0		0.26
GeO_2	expt	4.3930	4.3930	2.8626	90	90	90	55.244	1.8811	33.72		59.94	16.15		25.84	18.82	18.74			25.76
	calcd	4.4261	4.4261	2.8798	90	90	90	56.417	1.8961	43.50		57.65	16.89		19.51	18.39	18.43			27.92
	% error	0.68	0.68	0.60	0	0	0	2.1	0.80	29.0		−3.82	4.58		−24.5	−2.28	−1.65			8.39
TiO_2	expt	4.5930	4.5930	2.9590	90	90	90	62.422	1.9587	26.9		48.0	12.4		19.20	17.7	14.60			21.55
rutile	calcd	4.5718	4.5718	3.0046	90	90	90	62.799	1.9663	34.78		45.64	13.48		16.64	16.0	14.48			22.56
	% error	−0.46	−0.46	1.54	0	0	0	0.60	0.4	29.3		−4.9	8.71		−13.3	−9.5	−0.82			4.7
SnO_2	expt	4.7373	4.7373	3.1864	90	90	90	71.509	2.0535	26.17		44.96	10.31		20.74	17.72	15.55			21.23
cassiterite	calcd	4.7599	4.7599	3.1684	90	90	90	71.786	2.0572	30.21		42.14	12.55		18.47	18.79	13.13			21.30
	% error	0.48	0.48	−0.56	0	0	0	0.39	0.18	15.44		−6.3	21.73		−10.9	6.0	−15.6			0.33
ZrO_2	expt	5.1690	5.2320	5.3410	90	99.25	90	142.565	2.1661											
	calcd	5.2074	5.2135	5.2796	90	99.03	90	141.558	2.1647											
	% error	0.74	−0.35	−1.15	0	−0.22	0	−0.71	−0.06											
P_4O_{10}	expt	9.8257	9.8257	13.6455	90	90	120	1140.89	1.558											
	calcd	9.8298	9.8298	13.6315	90	90	120	1140.67	1.5454											
	% error	0.04	0.04	−0.1	0	0	0	−0.02	−0.8											
	% error	−0.04	−0.04	−0.04	0	0	0	−0.12	0.07											

TABLE 4: Structural and Mechanical Properties for Selected Crystal Silicates (Olevine)

		lattice parameters							elastic constants (10^{10} Pa)									
		a (Å)	*b* (Å)	*c* (Å)	α (deg)	V_{cell} (Å^3)	<Si−O>	<M−O>	<MI−O>	C_{11}	C_{22}	C_{33}	C_{44}	C_{55}	C_{66}	C_{12}	C_{13}	C_{14}	C_{23}	*B*
Mg_2SiO_4	expt	4.7530	10.1900	5.9780	90	289.5329	1.6352	2.1117		32.8	20.0	23.5	6.67	8.13	8.09	6.9	6.9		7.3	12.95
forsterite	calcd	4.8447	10.1875	6.0022	90	296.2444	1.6022	2.1126		29.82	17.46	21.6	3.87	5.85	6.82	6.94	7.41		7.44	11.99
	% error	1.9	−0.02	0.4	0	2.3	−2.0	0.04		9.1	−12.7	−8.0	−42.0	−28.0	−15.7	0.6	7.4		1.9	−7.41
Fe_2SiO_4	expt	4.8200	10.4790	6.0870	90	307.4469	1.6366	2.1649		26.6	16.8	23.2	3.23	4.65	5.70	9.40	9.20		9.20	13.4
fayalite	calcd	4.8727	10.2539	6.0564	90	302.6050	1.6024	2.1623		29.6	17.85	21.74	5.06	6.43	7.20	7.68	8.16		7.60	12.37
	% error	1.1	−2.1	−0.5	0	−1.6	−2.1	−0.1		11.3	6.3	−6.3	56.7	38	26.3	−18.3	−11.3		−17.4	−7.7
Mn_2SiO_4	expt	4.9020	10.5960	6.2570	90	324.999	1.6387	2.2129		25.84	16.56	20.68	4.53	5.56	5.78	8.70	9.50		9.20	12.8
tephroite	calcd	4.9834	10.5477	6.2537	90	328.717	1.6028	2.2390		22.79	13.29	17.16	3.94	5.25	5.80	6.08	6.43		5.99	9.56
	% error	1.66	−0.46	−0.05	0	1.14	−2.2	1.17		−11.8	−19.8	−17.0	−13.0	−5.6	0.3	−30.1	−32.3		−35	−25.3
$CaMgSiO_4$	expt	4.8220	11.1080	6.3820	90	341.838	1.6262	2.3703	2.1327	21.6	15.0	18.4	5.06	5.65	5.92	5.90	7.10		7.70	10.6
monticellite	calcd	4.8982	11.0653	6.3872	90	346.189	1.5992	2.3853	2.1353	21.24	13.58	17.56	4.26	5.36	5.63	6.56	7.55		7.2	10.19
	% error	1.58	−0.38	0.08	0	1.27	−1.66	0.63	0.12	−1.67	−9.47	−4.57	−15.8	−5.1	−4.9	11.2	6.3		−6.5	−3.9
Ni_2SiO_4	expt	4.7296	10.1209	5.9150	90	283.138	1.6396	2.0871		34.0	23.80	25.30	7.10	8.70	7.80	10.90	11.00		11.3	16.5
	calcd	4.8070	10.0909	5.9407	90	288.164	1.6026	2.119		33.06	19.75	23.82	4.07	6.41	7.51	7.74	8.29		8.16	13.35
	% error	1.6	−0.3	0.4	0	1.8	−2.3	1.5		−2.8	−17.0	−5.8	−42.7	−26	−3.7	−29	−24.6		−28	−19
Co_2SiO_4	expt	4.7820	10.3020	6.0030	90	295.733	1.6265	2.1305		30.78	19.47	23.42	4.67	6.39	6.48	10.2	10.5		10.3	14.8
	calcd	4.8483	10.2194	6.0025	90	297.404	1.6033	2.1481		28.6	16.15	20.8	2.04	5.20	6.22	6.05	6.66		7.03	11.16
	% error	1.38	−0.8	0.01	0	0.6	−1.4	0.8		−7.1	−17.1	−11.2	−56.3	−19	−4.0	−40.7	−36.6		−32	−24.6

variable potential model, but this choice would be very computationally expensive.

Bulk moduli for forsterite, fayalite, and monticellite are predicted with an error less than 10%, while for the other structures the bulk moduli are estimated within an error of about 20%. The typical errors for the elastic constants are of the same order of magnitude.

3.2.1.2 Garnets. The general formula for most of the garnets is $A_3B_2(SiO_4)_3$, where A represents a divalent metal such as calcium, iron, magnesium, or manganese placed in dodecahedral sites and B represents a trivalent metal such as aluminum, chromium, or iron placed in octahedral sites. Garnets are isostructural, meaning that they share the same crystal structure and belong to the isometric crystal class, which produces very symmetrical, cube-based crystals. We have considered four compounds, namely, $Mg_3Al_2Si_3O_{12}$ (pyrope), $Ca_3Al_2Si_3O_{12}$ (grossular), $Mn_3Al_2Si_3O_{12}$ (spessartite), and $Ca_3Fe_2Si_3O_{12}$ (andradite). Despite an error of about 2% for the Si−O average distance, the lattice vectors show a typical error less than 0.7%. The errors for the average distances of the divalent and trivalent cations with the oxygen are about 1.5%. A very good agreement is found for mechanical properties that have a typical error below 10% for all the crystals considered.

3.2.1.3. Phenacite. This class of mineral includes phenacite itself (Be_2SiO_4) and willemite (Zn_2SiO_4). Both the divalent cations and the silicon ions occupy tetrahedral sites. Results show that both the minerals are well reproduced, and in fact, typical errors are less than 0.5% for lattice parameters and the average divalent cation oxygen distances. The average Si−O distances are predicted with an error within 1.5%. Good agreement has been found with regards to the prediction of mechanical properties of phenacite, with errors below 10%. To our knowledge, no data are available for mechanical properties of willemite in the literature.

3.2.1.4. Zircon. The zircon structure also contains isolated silicate tetrahedra with zirconium 8-fold coordinated by the oxygen sublattice. The structure is tetragonal with the zirconium and silicon ions occupying special sites. In this case the structure is reproduced with errors below 1.7% while higher errors have been obtained in the calculation of mechanical properties such as C_{11} and C_{12} elastic constants.

3.2.1.5. Andalusite and Sillimanite. Typical errors of about 2% are found in lattice vectors and Si−O distances; however, it is noteworthy that the Al−O potential parameters that we have fitted for the octahedral sites in α-corundum are able to reproduce both the distances and the sites of the pentacoordinated and tetracoordinated Al cations in andalusite and sillimanite, respectively. Bulk moduli are predicted with an error of 5%, and most of the elastic constants are calculated with an error less than 10%.

3.2.2. Sorosilicates. Sorosilicates contain units made up of two tetrahedra that share one oxygen; the basic chemical unit is the anionic group $[Si_2O_7]^{6-}$. This structure forms an unusual hourglass-like shape. We have considered here the thortveitite mineral ($Sc_2Si_2O_7$, which features octahedral sites for Sc^{III} and a linear Si−O−Si bond between staggered tetrahedra), barylite ($BaBe_2Si_2O_7$), and hardystonite ($Ca_2ZnSi_2O_7$). The typical errors in the Si−O average distances are about 1.5%. An error of 2.8% is found for the *c*-axis in thortveitite, while for the other structures the cell parameters are predicted with errors less than 1.5%. The computed cell volume in hardystonite is greater than the experimental one because of the larger Ca−O distances (error 2.8%). Experimental mechanical properties are not available.

TABLE 5: Structural and Mechanical Properties for Selected Crystal Silicates (Garnets)

		lattice parameters								elastic constants (10^{10} Pa)										
		a (Å)	*b* (Å)	*c* (Å)	α (deg)	V_{cell} (Å^3)	<Si−O>	<Al/Fe−O>	<M−O>	C_{11}	C_{22}	C_{33}	C_{44}	C_{55}	C_{66}	C_{12}	C_{13}	C_{14}	C_{23}	*B*
$Mg_3Al_2Si_3O_{12}$ pyrope	expt	11.5480	11.5480	11.5480	90	1539.999	1.6361	1.8966	2.3007	29.62			9.00			11.11				17.28
	calcd	11.5515	11.5515	11.5515	90	1541.423	1.5942	1.9215	2.3195	26.68			8.57			11.76				16.73
	% error	0.03	0.03	0.03	0	0.09	−2.6	1.3	0.8	−9.9			−4.8			5.9				−3.2
$Ca_3Al_2Si_3O_{12}$ grossular	expt	11.8370	11.8370	11.8370	90	1658.536	1.6460	1.9237	2.4020	32.17			10.46			9.12				16.84
	calcd	11.9182	11.9182	11.9182	90	1692.918	1.6105	1.9663	2.4383	29.16			9.53			10.5				16.72
	% error	0.7	0.7	0.7	0	2.1	2.1	2.2	1.5	−9.4			−8.9			15.1				−0.7
$Mn_3Al_2Si_3O_{12}$ spessartite	expt	11.6190	11.6190	11.6190	90	1568.579	1.6398	1.9010	2.3252	30.95			9.52			11.35				17.88
	calcd	11.6935	11.6935	11.6935	90	1598.933	1.6003	1.9372	2.3654	26.92			9.52			10.78				16.16
	% error	0.6	0.6	0.6	0	1.94	−2.4	1.9	1.7	−13.0			0.0			−5.0				−9.6
$Ca_3Fe_2Si_3O_{12}$ andradite	expt	12.0310	12.0310	12.0310	90	1741.427	1.6409	2.0187	2.4252	28.9			8.5			9.2				15.7
	calcd	12.0665	12.0665	12.0665	90	1756.900	1.6039	2.0463	2.4539	28.02			8.0			9.19				15.47
	% error	0.3	0.3	0.3	0	0.9	−2.2	1.4	1.2	−3.0			−5.6			−0.1				−1.5

TABLE 6: Structural and Mechanical Properties for Selected Crystal Silicates (Other Important Nesosilicates)

		lattice parameters									elastic constants (10^{10} Pa)										
		a (Å)	*b* (Å)	*c* (Å)	α (deg)	*β* (deg)	*γ* (deg)	V_{cell} (Å^3)	<Si−O>	<M−O>	C_{11}	C_{22}	C_{33}	C_{44}	C_{55}	C_{66}	C_{12}	C_{13}	C_{14}	C_{23}	*B*
Be_2SiO_4 phenacite	expt	12.4720	12.4720	8.2510	90	90	120	1111.494	1.6323	1.6444	34.19		39.1	9.14			14.8	13.6	0.01		21.28
	calcd	12.4180	12.4180	8.2533	90	90	120	1102.208	1.6079	1.6504	34.92		38.35	9.64			14.63	12.34	0.05		20.75
	% error	−0.4	−0.4	−0.4	0	0	0	−0.8	−1.5	0.4	2.1		−1.9	5.5			−1.1	−9.2	400		−2.5
Zn_2SiO_4 willemite	expt	13.9480	13.9480	9.3150	90	90	120	1569.413	1.6346	1.9553											
	calcd	13.9012	13.9012	9.3093	90	90	120	1557.943	1.6082	1.9639											
	% error	−0.3	−0.3	−0.06	0	0	0	−0.7	−1.6	0.4											
$ZrSiO_4$ zircon	expt	6.6070	6.6070	5.9820	90	90	90	261.129	1.6223	2.1996	42.37		49.0	11.36			7.03	14.95			
	calcd	6.5654	6.5654	6.0777	90	90	90	261.979	1.5940	2.2358	52.74		46.0	10.19			11.31	13.75			25.42
	% error	−0.6	−0.6	1.6	0	0	0	0.3	−1.7	1.6	24.5		−6.1	−10.3			61	−8.0			
Al_2SiO_5 andalusite	expt	7.7942	7.8985	5.5590	90	90	90	342.226	1.6273	1.8834	23.34	28.9	38.01	9.95	8.78	11.23	9.77	11.62		8.14	16.20
	calcd	7.6678	7.9595	5.5203	90	90	90	336.920	1.5967	1.8927	20.0	25.0	35.4	8.97	6.67	12.26	10.27	12.05		10.9	15.4
	% error	−1.6	0.8	−0.7	0	0	0	−1.5	−1.9	0.5	−14.0	−13.6	−6.9	−9.8	−24	9.2	5.1	3.7		34	−5
Al_2SiO_5 sillimanite	expt	7.4856	7.6738	5.7698	90	90	90	331.435	1.6118	1.8526	28.73	23.19	38.84	12.24	8.07	8.93	15.86	8.3		9.47	17.1
	calcd	7.4001	7.4492	5.8238	90	90	90	321.037	1.5941	1.8487	30.04	25.16	39.87	12.26	7.77	8.35	10.22	11.44		16.48	18.07
	% error	−1.1	−2.9	0.9	0	0	0	3.1	−1.1	−0.2	4.6	8.5	2.7	0.2	−3.7	−6.5	−35.6	37.8		74	5.8

TABLE 7: Structural and Mechanical Properties for Selected Crystal Silicates (Sorosilicates)

		lattice parameters					<Si−O>	<M−O>	<MI−O>	elastic constants (10^{10} Pa)									
		a (Å)	*b* (Å)	*c* (Å)	*β* (deg)	V_{cell} (Å^3)				C_{11}	C_{22}	C_{33}	C_{44}	C_{55}	C_{66}	C_{12}	C_{13}	C_{14}	C_{23}	*B*
$Ca_2ZnSi_2O_7$	expt	7.8280	7.8280	5.0140	90	307.246	1.6213	2.5687	1.9372											
hardystonite	calcd	7.9470	7.9470	4.9981	90	315.658	1.5975	2.6315	1.9196											
	% error	1.5	1.5	−0.3	0	2.7	1.5	2.4	−0.9											
$Sc_2Si_2O_7$	expt	6.5030	8.4980	4.6820	102.77	252.339	1.6204	2.1217												
thortveitite	calcd	6.4429	8.4642	4.8141	102.78	256.026	1.6066	2.1461												
	% error	−0.9	−0.4	2.8	0.01	1.46	−0.85	1.15												
$BaBe_2Si_2O_7$	expt	9.8200	11.6700	4.6900	90	537.471	1.6316	2.9787	1.6456											
barylite	calcd	9.8738	11.7384	4.6178	90	535.217	1.6040	3.0102	1.6375											
	% error	0.5	0.6	1.5	0	−0.4	−1.7	1.1	−0.5											

3.2.3. Cyclosilicates. Cyclic metasilicates $[(SiO_3)_n]^{2n-}$ having 3, 4, 6, or 8 linked tetrahedra are known, 3 and 6 being the most common values. We have studied two three-membered ring silicates, namely, $Na_2Be_2Si_3O_9$ and $BaTi(SiO_3)_3$ (benitoite) and one six-membered ring silicate, $Al_2Be_3Si_6O_{18}$ (beryl). The $Na_2Be_2Si_3O_9$ structure is orthorhombic with Si_3O_9 rings parallel to the (010) direction. These rings are linked by Be_2O_6 groups, which comprise two BeO_4 tetrahedra sharing one edge. Sodium is heptacoordinated. The structure is well reproduced with typical errors within 1%. Larger errors are found in the benitoite structure where lattice parameters are 1% larger and the cell volume is expanded by 3.5%. The reason might be due to the fact that the Ba−O distances are too long (4.3%). Both structural parameters and mechanical properties are well predicted with typical errors within 1% and less than 10% for beryl, respectively.

3.2.4. Inosilicates. Chain metasilicates $[SiO_3^{2-}]_\infty$ formed by corner sharing of $[SiO_4]$ tetrahedra are particularly prevalent in many important minerals. Despite the apparent simplicity of the structural motif and stoichiometry, many different structures are encountered because of the different conformations that can be adopted by the linked tetrahedra. As a result, the repeat distance along the *c*-axis can be 2, 3, ..., 7, 9, or 12 tetrahedra. We have considered the pyroxene minerals enstatite ($Mg_2Si_2O_6$), jadeite ($NaAlSi_2O_6$), and spodumene ($LiAlSi_2O_6$), the synthetic metasilicates Li_2SiO_3 and Na_2SiO_3, and wollastonite ($Ca_2Si_3O_9$). Typical errors are within 2% for cell parameters and average distances, while calculated mechanical properties have higher errors with respect to the experimental ones.

3.2.5. Phyllosilicates. We have considered silicates with a layer structure of the formula $M_2Si_2O_5$ (M = Li, Na). Typical errors within 1.5% have been found in the structure. No experimental data are available for mechanical properties. It is worth noting that in these structures the ratio between the bridging oxygen and the nonbridging oxygen is 3:1 and the average Si−O distance is better reproduced, with an error within 1%. Despite the fact that $K_2Si_2O_5$ is not a phyllosilicate, we have added it in Table 10 because, as previously mentioned, the Li−O, Na−O, and K−O interactions have been parametrized using the structures of the alkali disilicate reported in Table 10.

3.2.6 Tectosilicates. We have considered two minerals, namely, $KAlSi_3O_8$ (microcline) and $NaAlSi_3O_8$ (albite), which are constructed from SiO_4 units with O atoms shared by two tetrahedra (as in the various forms of SiO_2 itself) and up to one-half of the Si atoms replaced by Al, thus requiring the addition of further cations to guarantee the electro-neutrality. In this case, the average Si−O distances are predicted with an error about 0.5%. The average Al−O distances are also reproduced with an error about 0.5%, while the errors in cell parameters are below 1.5%.

3.3. Glass Structure. Table 12 shows the comparison of bond length values obtained in this work with those obtained in previous simulations. Moreover, a comparison with the experimental results provided by neutron diffraction and EXAFS studies is also reported. The bond lengths have been calculated according to the method reported by Yuan and Cormack.[31] For the Si−O, O−O, and Si−Si pairs, the peak positions have been calculated by analyzing the full width at half-maximum (fwhm) of the calculated pair correlation functions broadened with Q_{max} = 45.2 Å^{-1}. The most probable distance of the Na−O pair distribution function has been taken as the bond length.

3.3.1. Local Structures in Sodium Silicate Glasses. Table 12 lists the results obtained by using the potentials derived in this

TABLE 8: Structural and Mechanical Properties for Selected Crystal Silicates (Cyclosilicates)

		lattice parameters								elastic constants (10^{10} Pa)										
		a (Å)	b (Å)	c (Å)	γ (deg)	V_{cell} (Å^3)	<Si−O>	<M−O>	<MI−O>	C_{11}	C_{22}	C_{33}	C_{44}	C_{55}	C_{66}	C_{12}	C_{13}	C_{14}	C_{23}	B
$Be_3Al_2(SiO_3)_6$	expt	9.2090	9.2090	9.1970	120	675.463	1.5974	1.6555	1.9163	30.85		28.34	6.61			12.89	11.85			18.10
beryl	calcd	9.2018	9.2018	9.2778	120	680.337	1.5922	1.6694	1.9459	30.28		28.12	4.69			13.01	11.06			17.59
	% error	−0.08	−0.08	0.88	0	0.7	−0.3	0.8	1.5	−1.8		−0.8	−29			0.9	−6.7			−2.8
$BaTi(SiO_3)_3$	expt	6.6410	6.6410	9.7600	120	372.776	1.6242	2.7668	1.9427											
benitoite	calcd	6.7157	6.7157	9.8804	120	385.913	1.6088	2.8857	1.9532											
	% error	1.1	1.1	1.2	0	3.5	−0.9	4.3	0.5											
$Na_2Be_2(SiO_3)_3$	expt	11.7480	9.4150	6.8180	90	754.121	1.6224	2.6314	1.6291											
	calcd	11.7355	9.4594	6.7974	90	754.583	1.6068	2.6649	1.6340											
	% error	−0.1	0.5	−0.3	0	0.06	−0.96	1.3	0.3											

TABLE 9: Structural and Mechanical Properties for Selected Crystal Silicates (Inosilicates)

		lattice parameters										elastic constants (10^{10} Pa)										
		a (Å)	b (Å)	c (Å)	α (deg)	β (deg)	γ (deg)	V_{cell} (Å^3)	<Si−O>	<Al−O>	<M−O>	C_{11}	C_{22}	C_{33}	C_{44}	C_{55}	C_{66}	C_{12}	C_{13}	C_{14}	C_{23}	B
$NaAlSi_2O_6$	expt	9.4180	8.5620	5.2190	90	107.97	90	400.315	1.6213	1.9273	2.4665	27.4	25.3	28.2	8.8	6.5	9.4	9.4	7.1		8.2	14.3
jadeite	calcd	9.4274	8.5110	5.2963	90	107.94	90	404.297	1.6016	1.9594	2.5034	25.59	25.86	28.18	9.43	7.27	5.99	8.17	8.16		11.3	14.84
	% error	0.1	−0.6	1.5	0	0.03	0	1.0	−1.2	1.67	1.5	−6.6	2.2	−0.07	7.2	11.8	−36	−13	15		38	3.8
$LiAlSi_2O_6$	expt	9.4630	8.3920	5.2180	90	110.15	90	389.017	1.6191	1.9208	2.2128	24.5	19.9	28.7	7.01	6.28	7.07	8.8	6.4		6.9	12.35
spodumene	calcd	9.4912	8.2439	5.3055	90	110.00	90	390.170	1.5992	1.9475	2.2293	24.83	20.57	26.66	9.63	10.28	4.87	9.82	11.78		10.96	14.95
	% error	0.3	−1.8	1.7	0	−0.16	0	0.3	−1.2	1.4	0.7	1.3	3.4	−7.1	37	64	−31	11.6	84		59	21.1
$Mg_2Si_2O_6$	expt	18.2350	8.8180	5.1790	90	90	90	832.764	1.6340		2.1149	22.47	17.79	21.36	7.76	7.59	8.16	7.24	5.41		5.27	10.78
estatite	calcd	18.5219	8.8489	5.2582	90	90	90	861.805	1.6054		2.0727	20.29	11.52	15.57	6.83	6.16	5.35	5.01	3.28		1.46	6.84
	% error	1.57	0.35	1.5	0	0	0	3.5	−1.75		−2.0	−9.7	−35	−27	−12	−19	−34	−31	−39		−72	−37
$Ca_3Si_3O_9$	expt	7.9400	7.3200	7.07	90.3	95.37	103.43	397.769	1.6227		2.4003											
wollastonite	calcd	7.8177	7.3330	7.126	90.1	92.82	103.54	396.641	1.6020		2.4454											
	% error	−1.5	0.18	0.8	−0.2	−2.7	0.1	−0.3	−1.3		1.9											
Na_2SiO_3	expt	10.4800	6.0700	4.8200	90	90	90	306.618	1.6381		2.3813											
	calcd	10.5754	5.9556	4.8264	90	90	90	304.039	1.6096		2.4039											
	% error	0.9	−1.9	0.1	0	0	0	−0.8	−1.7		0.9											
Li_2SiO_3	expt	9.3960	5.3960	4.6610	90	90	90	236.317	1.6408		2.0016											
	calcd	9.4656	5.3726	4.7286	90	90	90	240.470	1.6140		2.0406											
	% error	0.7	−0.4	1.45	0	0	0	1.8	−1.6		1.9											

TABLE 10: Structural and Mechanical Properties for Selected Crystal Silicates (Phyllosilicates)

		lattice parameters									elastic constants (10^{10} Pa)										
		a (Å)	*b* (Å)	*c* (Å)	α (deg)	*β* (deg)	*γ* (deg)	V_{cell} (Å^3)	<Si−O>	<M−O>	C_{11}	C_{22}	C_{33}	C_{44}	C_{55}	C_{66}	C_{12}	C_{13}	C_{14}	C_{23}	*B*
$Na_2Si_2O_5$	expt	6.4090	15.4220	4.8960	90	90	90	483.919	1.6160	2.3974											
	calcd	6.3042	15.4289	4.9626	90	90	90	482.698	1.6036	2.4116											
	% error	−1.6	0.04	1.36	0	0	0	−0.25	−0.76	0.6											
$Li_2Si_2O_5$	expt	5.6830	4.7840	14.6480	90	90	90	398.242	1.6182	1.9987											
	calcd	5.6244	4.8754	14.6526	90	90	90	401.793	1.6054	2.0181											
	% error	−1.0	1.9	0.03	0	0	0	0.9	−0.8	0.97											
$K_2Si_2O_5$[a]	expt	16.3224	11.2430	9.9190	90	115.97	90	1636.459	1.6235	2.8500											
	calcd	16.4127	11.2904	9.8247	90	114.16	90	1661.119	1.6061	2.8952											
	% error	0.6	0.4	−0.95	0	−1.6	0	1.5	−1.07	1.6											

[a] $K_2Si_2O_5$ is not a phyllosilicate, we have included it here because, as previously mentioned, the Li−O, Na−O, and K−O interactions were parametrized using the structures of the alkali disilicate.

TABLE 11: Structural and Mechanical Properties for Selected Crystal Silicates (Tectosilicates)

		lattice parameters										elastic constants (10^{10} Pa)										
		a (Å)	*b* (Å)	*c* (Å)	α (deg)	*β* (deg)	*γ* (deg)	V_{cell} (Å^3)	<Si−O>	<Al−O>	<M−O>	C_{11}	C_{22}	C_{33}	C_{44}	C_{55}	C_{66}	C_{12}	C_{13}	C_{14}	C_{23}	*B*
$KAlSi_3O_8$	expt	7.9205	7.6219	7.2188	76.55	104.38	66.87	360.56	1.6446	1.6557	2.9262	6.7	16.9	11.8	1.43	2.38	3.64	4.53	2.65		2.04	5.54
microcline	calcd	7.7892	7.5786	7.2248	78.95	105.56	61.6	334.79	1.6360	1.6468	2.9378	13.96	7.72	13.13	3.47	2.79	3.31	4.12	2.87		3.07	4.41
	% error	−1.66	−0.57	0.08	3.1	1.1	−7.9	−7.1	−0.5	−0.5	0.4	108	−54	11.3	142	17.2	−9.1	−9.1	8.3		50.5	−20
$CaAl_2Si_2O_8$	expt	8.1750	12.8730	14.1700	93.11	115.89	91.28	1337.804	1.6209	1.7412	2.4982	12.4	20.5	15.6	2.35	4.04	4.15	6.6	5.0		4.2	8.42
anorthite	calcd	7.9151	12.9053	14.0846	93.49	115.68	91.67	1291.74	1.5989	1.7302	2.4837	10.0	18.0	17.17	3.61	3.75	3.12	4.94	6.33		4.32	7.73
	% error	−3.1	0.25	−0.6	0.4	−0.2	0.4	−3.4	−1.35	−0.6	−0.6	−19.3	−12.	10.0	53.6	−7.2	−25	−25	26.6		2.9	−8.2
$NaAlSi_3O_8$	expt	8.1520	12.8310	7.1100	93.46	116.52	89.72	664.026	1.6391	1.6391	2.5290	7.40	13.1	12.8	1.73	2.96	3.20	3.64	3.94		3.1	5.69
albite	calcd	8.0500	12.6704	7.0210	93.46	116.52	89.72	639.404	1.6312	1.6312	2.5298	6.67	16.1	15.36	1.66	3.49	2.94	3.46	4.70		1.1	5.46
	% error	−1.25	−1.25	−1.25	0	0	0	−3.7	−0.5	−0.5	0.03	−9.9	22.9	20	−4.0	17.9	−8.1	−4.9	19		−63	−4.0

TABLE 12: Comparison of Bond Lengths of the Simulated Glasses with Different Interatomic Potentials and Experimental Studies

	Na_2O %	MD this work[a]	MD Du[b]	MD Yuan[c]	neutron[d]	EXAFS[e]
Si−O	$x = 0$	1.616	1.620/1.619	1.616/1.615	1.610/1.608	1.608
	$x = 10$	1.618	1.615	1.615		
	$x = 15$	1.617				
	$x = 20$	1.616	1.615	1.614	1.617	1.617
	$x = 25$	1.615				
	$x = 30$	1.614	1.611	1.613	1.622	1.668
Si−BO/Si−NBO	$x = 0$	1.616				
	$x = 10$	1.621/1.550				
	$x = 15$	1.622/1.553				
	$x = 20$	1.624/1.554				
	$x = 25$	1.626/1.556				
	$x = 30$	1.628/1.559				
O−O	$x = 0$	2.624	2.624/2.617	2.626/2.621	2.629/2.626	
	$x = 10$	2.626	2.628	2.622		
	$x = 15$	2.624				
	$x = 20$	2.624	2.624	2.622		
	$x = 25$	2.624				
	$x = 30$	2.623	2.624	2.608		
Si−Si	$x = 0$	3.140	3.146/3.159	3.129	3.077/3.077	
	$x = 10$	3.149	3.146	3.140		
	$x = 15$	3.146				
	$x = 20$	3.150	3.142	3.142		
	$x = 25$	3.148				
	$x = 30$	3.149	3.146	3.139		
Na−O	$x = 10$	2.307	2.362	2.31		2.32
	$x = 15$	2.288				
	$x = 20$	2.312	2.382	2.32	2.36	2.30
	$x = 25$	2.332				
	$x = 30$	2.323	2.388	2.33	2.36	

[a] Results obtained using the interatomic potential developed in this work. The values listed are an average upon three simulations starting from different initial configurations. [b] Data from Du and Cormack.[43] [c] Data from Yuan and Cormack.[31] [d] Neutron diffractions are from Wright et al.[52] and Clare et al.[55] with Q_{max} of 22.88 Å^{-1}, and that of silica is from Grimley et al.[54] with Q_{max} of 45.2 Å^{-1} and where indicated after the slash.[e] Si−O bond lengths are from Henderson;[56] Na−O data are from Greaves et al.[57] and Mazzara et al.[58]

work and those obtained by Cormack et al.[31,43] by making use of the Buckingham function and the same ionic charge scheme adopted in this work. Our results agree with those obtained by Cormack et al.,[31,43] for both the short-range and the medium-range orders with respect to the Si−O backbone network structure. All the simulations reported in Table 12 predict that the average Si−O bond length become shorter by increasing the sodium content in the glass. The Si−O bond length decreases slightly from 1.618 to 1.614 Å passing from NS10 to NS30. This result apparently contradicts the experimental data obtained from neutron diffraction experiments by Wright et al.[53] They found that the Si−O bond length increases from 1.617 to 1.622 Å for glasses with 22 and 31 mol % Na_2O concentrations, respectively. We note, however, that although the average Si−O bond length decreases, both Si−NBO and Si−BO bond lengths increase with sodium concentration: The Si−BO bond length increases from 1.621 to 1.628 Å, while the Si−NBO bond length increases from 1.550 to 1.559 Å. The Si−NBO distance is nearly 0.069 Å shorter than the Si−BO bond lengths. These findings are in agreement with the differences of Si−BO and Si−NBO bond lengths in the α-$Na_2Si_2O_5$ and Na_2SiO_3 crystal phases, which are 0.06 and 0.08 Å, respectively.[59] The average Si−O bond length decreases because the NBO content increases with Na concentration and the increase of the bond length values of both components is not sufficient to invert the trend. In fact, the intensity of the BO peaks decreases while, at the same time, the NBO peak increases. These observations were attributed by Yuan and Cormack to the lack of distinct charge assignments for BO and NBO in the potential model.[31] This trend is found also in modeling silicate crystals, as discussed previously in section 3.2.1.1. In fact, the negative errors associated with the Si−O bond lengths decrease from 2% in nesosilicates to 0.5% in tectosilicates. The error increase depends on the increase of the NBO/BO ratio in the system. The addition of sodium oxide produces an increase of the ionic character of the Si−O bond, and it could be more appropriate to use a variable charge potential model[15] to reproduce the experimental data.

The O−O bond length is 2.624 Å and does not seem to change with the addition of sodium oxide. This value is in agreement with the neutron diffraction data of 2.629 Å.[53]

The Na−O bond lengths range from 2.300 to 2.332 Å, and the pair distribution function shows that the Na−O peak increases and becomes sharper with the addition of Na_2O (Figure 1a). These results agree well with EXAFS and neutron diffraction data for which the Na−O bond lengths range from 2.30 to 2.36 Å.[55,57,58]

The coordination number of the sodium ions increases from 4.32 to 4.78 for NS10 and NS30 glasses, and it tends to 5 for the $Na_2Si_2O_5$ glass (Table 13). Accordingly, Greaves et al.[56] also found that 5 ± 0.5 O ions are around Na for sodium disilicate glasses.

The NBO/BO ratio around Na increases with the sodium oxide content, it ranges from 0.82 to 2.14, and the BO/NBO ratio around Si is 3.65 for NS30 glass, while both the ratio values are 4 in the crystalline $Na_2Si_2O_5$.[59]

All these observations show that the average local environment around the Na ions becomes more ordered with the addition of Na_2O. This is demonstrated also by analyzing the O−Na−O bond angle distribution, Figure 1b. As already discussed by Cormack et al.,[31,43] this distribution features a distinct peak at 60°, a broad peak at around 90°, and a shoulder at 150°.

Table 14 reports peak positions and fwhm's of O−Si−O and Si−O−Si bond angle distributions. The O−Si−O angle in-

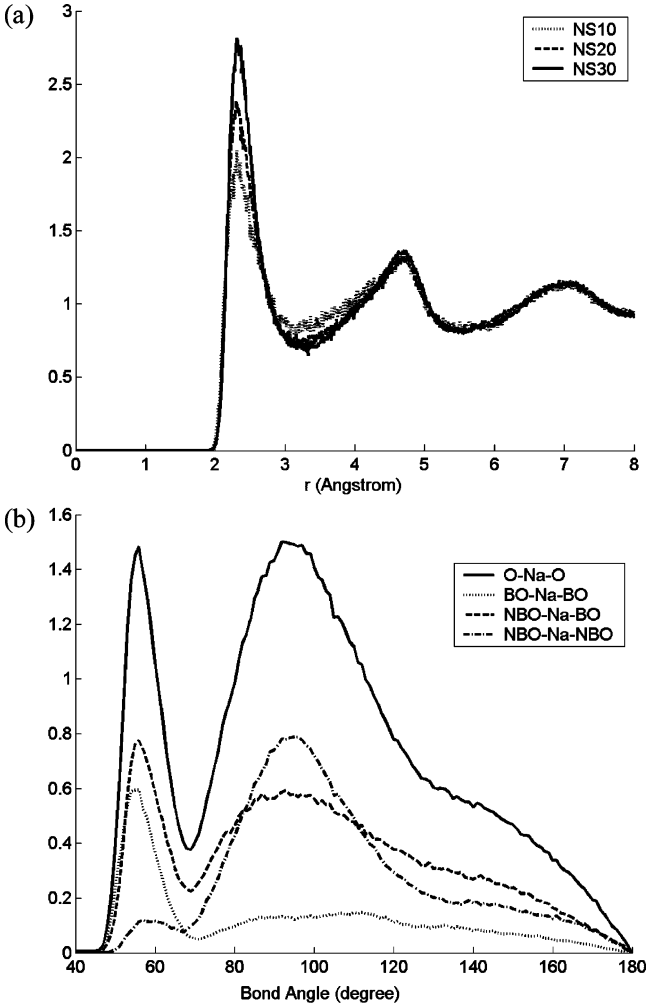

Figure 1. (a) Na−O pair distribution functions for the sodium silicate glasses simulated. We have reported only the NS10, NS20, and NS30 glasses for clarity (b) Bond angle distribution function O−Na−O for NS30 glass and BO and NBO contributions.

TABLE 13: Coordination Numbers and Their BO and NBO Contributions[a]

	NS10	NS15	NS20	NS25	NS30
Si−O	4.00	4.00	4.00	4.00	4.00
Si−BO	3.78	3.65	3.50	3.33	3.14
Si−NBO	0.22	0.35	0.50	0.67	0.86
Na−O	4.32	4.46	4.60	4.71	4.78
Na−BO	2.37	2.02	1.88	1.68	1.52
Na−NBO	1.95	2.44	2.72	3.03	3.26

[a] The cutoffs were set to 1.8 and 3.0 Å for the Si−O and Na−O pairs, respectively.

TABLE 14: Bond Angle Distributions of Silica and Sodium Silicate Glasses

	O−Si−O (deg)		Si−O−Si (deg)	
	peak	fwhm	peak	fwhm
SiO_2	108.6	13.5	153.5	34
NS10	108.7	13.0	153.6	34.5
NS15	108.8	12.7	152.7	33.5
NS20	108.9	12.2	152.8	32.5
NS25	109.0	12.0	151.0	33.8
NS30	109.0	11.3	150.6	33.7

creases from 108.6° for silica to 109.0° for NS30 glass, while the fwhm decreases from 13.5° to 11.2°. These results agree well with those obtained by means of neutron diffraction studies by Mitsawa et al.[64] They reported a slight increase of the O−Si−O angle from 109.1° for silica to 109.3° for sodium disilicate glass. The SiO_4 tetrahedra reach a more regular geometry when the network is depolymerized.

To our knowledge no experimental data are available for the Si−O−Si angle distribution in sodium silicate glasses. High-energy X-ray studies of silica[65] show the Si−O−Si peak position and fwhm to be 147° and 35°, respectively, in agreement with the results of two-dimensional ^{17}O dynamic-angle spinning NMR[66] spectroscopy, which estimated the peak position of the Si−O−Si angle to be 146.7° ± 3.8°. The results obtained in this study show that the peak positions of the Si−O−Si bond angle distribution decreases from 153.5° for silica to 150.6° for NS30 glass. As previously suggested, the overestimation of this angle might be due to the limited size of the simulation box utilized and lack of polarizability effects in the calculations.[18]

3.3.2. Mechanical Properties.. Table 15 lists the *E*, *G*, *B*, and ν values obtained in this work by averaging upon three simulation runs, together with those predicted using the different empirical methods included into the SciGlass package[49] and together with experimental data.[47] The percent errors are reported in brackets. We have chosen the empirical models that provide the best agreement with the experimental data. These are incremental models, valid within limited concentration ranges, namely, Appen's method,[67] Gan Fuxi's method,[68] Demkina's method,[69] and Priven's method.[70]

The agreement of the results obtained from the simulations with the experimental data is good. The Young's modulus decreases upon the addition of sodium oxide because of the decrease in the polymerization of the silica network. In fact, the elastic modulus *E* is determined by the individual bonds in the material and by the structure of the network (intermediate range order). The shear modulus *G* decreases with Na_2O concentration, and it is slightly underestimated, as is the Young modulus *E*. However, in both cases the errors are within 6%. However, both the bulk modulus and the Poisson's ratio increase with Na_2O concentration. This might be due to the fact that upon the addition of Na_2O the total free volume decreases, while the density of packing of the atoms in the structure increases leading to a lower compressibility of the material and to a higher bulk modulus. The relative errors of both *B* and ν are overestimated by 7% and 15%, respectively.

3.4. Alumino-Phosphate. A good test for the transferability of a new interatomic potential is to compare the computed structural and mechanical properties of a compound that has not been explicitly considered during the parametrization procedure. We have chosen the alumino-phosphate $AlPO_4$ berlinite because of its interest and of the presence of previous calculations with different potential models.[38,39,71] In fact, in the past few decades, many researchers focused their attention on the wide class of zeolite minerals. Their rich polymorphism, combined with their technological importance as selective catalysts and adsorbents, has induced a widespread interest in the physical and chemical properties of these systems. Therefore, nowadays many force fields are available in the literature.[38,39,71]

Table 16 reports the structural and mechanical properties and static dielectric constants calculated using the force field derived in this study. They are compared with experimental data[72−74] and with the results calculated by means of two of the force fields more widely used. Gale and Henson[39] used Buckingham functions and treated the polarizability of the oxygen atoms using the shell model developed by Dick and Overhauser.[75] They used Catlow's parameters[76] for the O−O interaction and derived the P−O parameters by empirical fitting of the crystal structure and the elastic and dielectric properties of berlinite. Kramer et

TABLE 15: Comparison of Mechanical Properties (E = Young's Modulus, G = Shear Modulus, B = Bulk Modulus and ν = Poisson's Ratio) Calculated by Means of Free Energy Minimizations (T = 300 K and P = 1 atm) with Experimental Data from Ref 47 and Those Predicted by Means of Different Empirical Methods Available in the SciGlass Package[49]

	Na_2O %	experimental	this work	Appen	Demkina 76	Gan Fuxi	Priven 2000
E (GPa)	$x = 0$	72.50[a]	72.05 (−0.6)	70.24 (−3.1)	66.42 (−8.4)	71.83 (−0.9)	68.00 (−6.2)
	$x = 10$	65.29	64.20 (−1.7)	66.06 (1.2)	66.27 (1.5)	67.05 (2.7)	59.30 (−9.2)
	$x = 15$	62.90	61.07 (−2.9)	64.12 (1.9)	66.19 (5.2)	64.85 (3.1)	62.45 (−0.7)
	$x = 20$	61.08	58.53 (−4.2)	62.27 (1.9)	66.09 (8.2)	62.76 (2.8)	60.60 (−0.8)
	$x = 25$	59.77	58.13 (−2.7)	60.53 (1.3)	65.99 (10.4)	60.80 (1.7)	58.75 (−1.7)
	$x = 30$	59.33	56.64 (−4.5)	58.58 (−1.3)	65.88 (11.0)	58.96 (−0.6)	56.90 (−4.1)
G (GPa)	$x = 0$	31.25[a]	30.43 (−2.6)	29.72 (−4.9)	28.49 (−8.8)	31.18 (−0.2)	29.06 (−7.0)
	$x = 10$	27.68	26.99 (−2.5)	27.34 (−1.2)	28.15 (1.7)	28.48 (2.9)	24.87 (−10.2)
	$x = 15$	26.29	25.11 (−4.5)	26.22 (−0.3)	27.98 (6.4)	27.23 (3.6)	26.19 (−0.4)
	$x = 20$	25.18	23.60 (−6.3)	25.15 (−0.1)	27.81 (10.4)	26.04 (3.4)	25.27 (−0.4)
	$x = 25$	24.26	23.26 (−4.1)	24.13 (−0.5)	27.65 (14.0)	24.91 (2.7)	24.36 (−0.4)
	$x = 30$	23.80	22.38 (−6.0)	23.16 (−2.7)	27.48 (15.5)	23.85 (0.2)	23.46 (−1.4)
B (GPa)	$x = 0$	36.10[a]	37.94 (5.1)	36.76 (1.8)	33.11 (−8.3)	34.41 (−4.7)	34.34 (−4.9)
	$x = 10$	33.95	34.67 (2.1)	37.72 (11.1)	34.20 (0.7)	34.62 (2.0)	34.08 (0.4)
	$x = 15$	34.51	35.57 (3.1)	38.52 (11.6)	34.76 (0.7)	34.96 (1.3)	33.84 (−1.9)
	$x = 20$	35.46	37.18 (4.9)	39.60 (11.7)	35.32 (−0.4)	35.48 (0.0)	33.58 (−5.0)
	$x = 25$	37.16	38.52 (3.7)	41.02 (10.4)	35.88 (−3.4)	36.22 (−2.5)	33.30 (10.4)
	$x = 30$	39.03	40.13 (2.8)	42.87 (9.8)	36.46 (−6.6)	37.22 (−4.6)	33.02 (−15.4)
ν	$x = 0$	0.160[a]	0.184 (15.0)		0.166 (3.8)		0.170 (6.3)
	$x = 10$	0.180	0.191 (6.1)		0.177 (−0.3)		0.186 (3.3)
	$x = 15$	0.196	0.216 (10.2)		0.183 (−6.6)		0.192 (−2.0)
	$x = 20$	0.213	0.240 (12.7)		0.188 (−11.7)		0.199 (−6.6)
	$x = 25$	0.232	0.250 (7.8)		0.194 (−16.4)		0.206 (−11.2)
	$x = 30$	0.247	0.265 (7.3)		0.199 (−19.4)		0.213 (−13.8)

[a] Elastic constants for SiO_2 glass have been taken from ref 48, and G was calculated by means of eq 9.

TABLE 16: Comparison of Experimental and Calculated Structures and Properties for $AlPO_4$ Berlinite with Different Potential Models (T = 300K and P = 1 atm)

	exptl[a]	Gale and Henson[39]	Kramer et al.[38]	this work
a (Å)	4.9423	4.9117	5.0111	4.9448
c (Å)	10.9446	10.9576	11.1424	10.9833
Al, x	0.4664	0.4671	0.4672	0.4547
P, x	0.4669	0.4699	0.4656	0.4541
O(1), x	0.4163	0.4083	0.4331	0.4308
O(1), y	0.2922	0.2890	0.2907	0.3043
O(1), z	0.3977	0.4973	0.4035	0.3983
O(2), x	0.4156	0.4179	0.4232	0.4172
O(2), y	0.2576	0.2599	0.2486	0.2639
O(2), z	0.8837	0.8823	0.8903	0.8851
<Al−O>	1.7358	1.7351	1.7398	1.7339
<P−O>	1.5213	1.5212	1.5081	1.5194
V_{cell} (Å^3)	231.5201	228.9378	242.3105	232.5725
C_{11} (10^{10} Pa)	6.98	8.19	8.40	6.92
C_{33} (10^{10} Pa)	8.71	10.69	9.69	10.18
C_{44} (10^{10} Pa)	4.22	4.41	4.68	3.98
C_{12} (10^{10} Pa)	1.06	1.59	0.93	1.24
C_{13} (10^{10} Pa)	1.49	2.22	1.57	1.41
C_{14} (10^{10} Pa)	1.34	1.09	1.35	1.28
B (10^{10} Pa)	3.39	4.25	3.81	3.46
ϵ^0_{11}	5.47	5.25	1.92	2.08
ϵ^0_{33}	5.37	5.42	1.94	2.11

[a] The trigonal symmetry class with space group $P3_121$ has been taken from Thong and Schwarzenbach;[72] mechanical properties based on Brillouin scattering are from ref 73, and static dielectric constants are from ref 74.

al.[38] used a rigid ionic model with partial charges, and the parameters of the Buckingham functional form for the short-range interactions were derived by fitting to the potential energy surface of small clusters of H_4TO_4 (T = Si, Al, P) to represent the building blocks of zeolites.

Despite the fact that our potentials were derived by empirical fitting of crystal structures and elastic properties of binary oxides (α-Al_2O_3 and P_4O_{10} for Al−O and P−O interactions, respectively), our results on berlinite structural and mechanical properties are similar to those calculated with Kramer's potentials. Both Kramer's potentials and our force field fail in simulating dielectric properties because they adopt the rigid ionic model. However, even within this approximation, structural and mechanical properties are in good agreement with experimental data and with those calculated with the potential developed by Gale and Henson.

4. Conclusions

A self-consistent pairwise interatomic potential has been developed by means of empirical fitting on structural parameters and elastic constants of binary oxides using free energy minimization at T = 300 K and P = 1 atm.

A rigid ionic potential model has been used, and a partial charge $q_O = -1.2e$ has been assigned to the oxygen atom. Despite the fact that the O−O interaction has been fitted on α-quartz, this provides good results also for other oxides in which different covalency is present. These differences are subsumed in the M−O parameters that were subsequently fitted on binary oxides.

The potential derived in this work has been shown to be able to reproduce structural parameters and mechanical properties of a wide range of crystal silicates and glasses.

The Si−O average distances have been found to be shorter than the experimental ones in all the cases that we have studied, and the errors increase with the NBO/BO ratio in the glasses. This result is expected, since the Si−O interaction has been derived from α-quartz that is a tectosilicate with no NBO oxygens. The potential model could be improved by taking into account different charges for bridging and nonbridging oxygens in a variable charge potential model.

Thanks to the choice of a pairwise partial charge model, the computational effort required in the evaluation of forces is reduced with respect to a three-body term potential, a variable charge model,[14,15] or a core−shell model.[71] In addition, no assumptions are made about the coordination number of the

cations. In fact, since a two-body potential is employed, the cations are allowed to change their coordination depending on the environment in which they are placed. For instance, the Al−O interaction has been parametrized on corundum in which Al is 6-fold coordinated with average bond length distances of 1.913 Å. However, the environment around Al is well reproduced both in $AlPO_4$ berlinite in which Al is 4-fold coordinated and other alumino-silicates in which Al can occupy 4-, 5-, and 6-fold sites.

The force field that we have obtained in this work could be further refined by considering additional properties besides structural end elastic parameters, but the choice can be hindered by the availability of experimental data. However, ab initio simulation of complex materials has now reached a level of excellent accuracy not only with respect to structures but also as far as dynamical features are concerned, such as vibrational frequencies.[77,78] Therefore, it could be possible, in the future, to consider also this a source of accurate data to refine classical force fields.

Finally, the calculations performed on the sodium silicate glass are very promising; further work has been devoted to similar alkaline silicate glasses, and it will be reported in near future. Moreover, it is worth noting that the potential derived in this study is able to reproduce structural and mechanical properties of alumino-phosphates, although they have not explicitly considered during the parametrization procedure.

Acknowledgment. This work was supported by Ministero dell'Istruzione, Università e Ricerca, (Grant No. 2003032158_005). We gratefully acknowledge Professor Julian Gale for his kindness and his very helpful advice for using the GULP package.

References and Notes

(1) Shelby, J. E. *Introduction to Glass Science and Technology*, 2nd ed.; Royal Society of Chemistry: Cambridge, U. K., 2005.
(2) Catlow, C. R. A.; Cormack, A. N.; Theobald, F. *Acta Crystallogr., Sect. B* **1984**, *40*, 195.
(3) Dove, M. T. *Introduction to Lattice Dynamics*; Cambridge University Press: New York, 2005.
(4) Allen, M. P.; Tildsley, D. J. *Computer Simulation of Liquids*; Oxford University Press: Oxford, U. K., 1987.
(5) Oganov, A. R.; Brodholt, J. P.; Price, G. D. *Phys. Earth Planet. Inter.* **2000**, *122*, 277.
(6) Purton, J.; Jones, R.; Catlow, C. R. A.; Leslie, M. *Phys. Chem. Miner.* **1993**, *19*, 392.
(7) Jund, P.; Jullien, R. *Phys. Rev. B* **1999**, *59*, 13707.
(8) Van Beest, B. W. H.; Kramer, G. J.; Van Santen, R. A. *Phys. Rev. Lett.* **1990**, *64*, 1955.
(9) Duffrene, L.; Kieffer J. *J. Phys. Chem. Solids* **1998**, *59*, 1025.
(10) Demilrap E.; Cagin T.; Goddard W. A. *Phys. Rev. Lett.* **1999**, *82*, 1708.
(11) Vashishta, P.; Kalia, R. K.; Rino, J. P.; Ebbsjo, I. *Phys. Rev. B* **1990**, *41*, 12197.
(12) Takada, A.; Richet, P.; Catlow, C. R. A.; Price, G. D. *J. Non-Cryst. Solids* **2004**, *345/346*, 224.
(13) Chagarov, E.; Adams, J. B.; Kieffer, J. *Modell. Simul. Mater. Sci. Eng.* **2004**, *12*, 337.
(14) Huff, N. T.; Demiralp, E.; Cagin, T.; Goddard, W. A., III. *J. Non-Cryst. Solids* **1999**, *253*, 133.
(15) Rappe A. K.; Goddard, W. A., III. *J. Phys. Chem.* **1991**, *95*, 3358.
(16) Wilson, M.; Madden, P. A.; Hemmati, M.; Angell, C. A. *Phys. Rev. Lett.* **1996**, 77, 4023.
(17) Wilson, M.; Madden, P. A.; Costa-Cabral, B. J. *J. Phys. Chem.* **1996**, *100*, 1227.
(18) Wilson, M.; Walsh, T. R. *J. Chem. Phys.* **2000**, *113*, 9180.
(19) Walsh, T. R.; Wilson, M.; Sutton, A. P. *J. Chem. Phys.* **2000**, *113*, 9191.
(20) Tilocca, A.; de Leeuw, N. H.; Cormack, A. N. *Phys. Rev. B* **2006**, *73*, 104209.
(21) *Cerius2*, version 4.2; Accelrys: San Diego, CA, 2000.
(22) Garofalini, S. H. In *Molecular Modelling Theory: Applications in the Geosciences*; Cygan, R. T., Kubicki, J. D., Eds.; Reviews in Mineralogy Geochemistry 42; Geochemical Society, Mineralogical Society of America: Washington, DC, 2001; Chapter 5 and references therein.
(23) Zachariasen, W. H. *J. Am. Chem. Soc.* **1932**, *54*, 3841.
(24) Bush, T. S.; Gale, J. D.; Catlow, C. R. A.; Battle, P. D. *J. Mater. Chem.* **1994**, *4*, 831.
(25) Lewis, G. V.; Catlow, C. R. A. *J. Phys. C: Solid State Phys.* **1985**, *18*, 1149.
(26) Vessal, B.; Amini, M.; Fincham, D.; Catlow, C. R. A. *Philos. Mag. B* **1989**, *60*, 753.
(27) Lusvardi, G.; Malavasi, G.; Menabue, L.; Menziani, M. C. *J. Phys. Chem. B* **2002**, *106*, 9753.
(28) Linati, L.; Lusvardi, G.; Malavasi, G.; Menabue, L.; Menziani, M. C.; Mustarelli, L. P.; Segre, U. *J. Phys. Chem. B* **2005**, *109*, 4989.
(29) Lusvardi, L.; Malavasi, G.; Menabue, L.; Menziani, M. C.; Pedone, A.; Segre, U. *J. Phys. Chem. B* **2005**, *109*, 21586.
(30) Malavasi, G.; Menziani, M. C.; Pedone, A.; Segre, U. *J. Non-Cryst. Solids* **2006**, *352*, 285.
(31) Yuan, X.; Cormack, A. N. *J. Non-Cryst. Solids* **2001**, *283*, 69.
(32) Corradi, A. B.; Cannillo, V.; Montorsi, M.; Siligardi, C.; Cormack, A. N. *J. Non-Cryst. Solids* **2005**, *351*, 1185.
(33) Parker, S. C.; Price G. D. *Adv. Solid State Chem.* **1989**, *1*, 295.
(34) Gale, J. D. *J. Chem. Soc., Faraday Trans.* **1997**, *93*, 629.
(35) Gale J. D. *Philos. Mag. B* **1996**, *73*, 3.
(36) The General Utility Lattice Program by J. Gale can be downloaded from the Web site http://gulp.curtin.edu.au/.
(37) Gale, J. D.; Rohl, A. L. *Mol. Simul.* **2003**, *29*, 291.
(38) Kramer, G. J.; Farragher, N. P.; van Beest, B. W. H.; van Santen, R. A.; *Phys. Rev. B* **1991**, *43*, 5068.
(39) Gale, J. D.; Henson, N. J. *J. Chem. Soc., Faraday Trans.* **1994**, *90*, 3175.
(40) atson, G. W.; Tschaufeser, P.; Wall, A.; Jackson, R. A.; Parker, S. C. In *Computer Modelling in Inorganic Crystallography*; Catlow, C. R. A., Ed.; Academic Press: San Diego, CA, 1997; Chapter 3.
(41) Ney, J. F. *Physical Properties of Crystals*; Oxford Scientific Publications: Oxford, U. K., 1985.
(42) Bakaev, V. A.; Steele, W. A. *J. Chem. Phys.* **1999**, *111*, 9803
(43) Du, J.; Cormack, A. N. *J. Non-Cryst. Solids* **2004**, *349*, 66.
(44) Ewald P. P. *Ann. Phys.* **1921**, *64*, 253.
(45) Leach, A. R. *Molecular Modelling: Principles and Applications*; Prentice Hall: New York, 2001.
(46) Fletcher, R.; Reeves, C. M. *Comput. J.* **1964**, *7*, 149.
(47) Manghnani, M. H. In *Handbook of Glass Properties*; Bansal, N. P., Doremus, R. H., Eds.; Academic Press: London, 1986.
(48) Hwa, L. G.; Hsieh, K. J.; Liu, L. C. *Mater. Chem. Phys.* **2003**, *78*, 105.
(49) *SciGlass, Universal System of Glass Properties*, version 3.5; SciVision: Burlington, MA, 1997 and references therein.
(50) The DL_POLY code by W. Smith and T. R. Forester can be downloaded from the Web site http://www.dl.ac.uk/TCSC/Software/DL_POLY.
(51) Evans, D. J. Morris, G. P. *Comput. Phys. Rep.* **1984**, *1*, 297.
(52) Yuan, X.; Cormack, A. N. *Comput. Mater. Sci.* **2002**, *24*, 343.
(53) Wright, A. C.; Clare, A. G.; Bachra, B.; Sinclair, R. N.; Hannon, A. C.; Vessal, B. *Trans. Am. Crystallogr. Assoc.* **1991**, *27*, 239.
(54) Grimley, D. I.; Wright, A. C.; Sinclair, R. N. *J. Non-Cryst. Solids* **1990**, *119*, 49.
(55) Clare, A. G.; Bachra, B.; Wright, A. C.; Sinclair, R. N. In *The Physics of Non-Crystalline Solids*; Pye, L. D., Lacourse, W. C., Stevens, H. J., Eds.; Taylor and Francis: London, 1992.
(56) Henderson, G. S. *J. Non-Cryst. Solids* **1995**, *183*, 43.
(57) Greaves, G. N.; Fontaine, A.; Lagrarde, P.; Raoux, D.; Gurman, S. J. *Nature* **1981**, *293*, 611.
(58) Mazzara, C.; Jupille, J.; Flank, A. M.; Lagarde, P. *J. Phys. Chem B* **2000**, *104*, 3438.
(59) *Inorganic Crystal Structure Database*, version 1.3.3; National Institute of Standards and Technology: Gaithersburg, MD, 2004 and references therein.
(60) Ozkan, H.; Cartz, L.; Jamieson, J. C. *J. Appl. Phys.* **1974**, *45*, 556.
(61) Lide, D. R. *Handbook of Chemistry and Physics*, 76th ed.; CRC Press: Boca Raton, FL, 1995−1996.
(62) Born, M.; Huang, K. *Dynamical Theory of Crystal Lattices*; Clarendon Press: Oxford, U. K., 1954.
(63) Bass, J. D. Chapter 7 In *Mineral Physics and Crystallography: A Handbook of Physical Constants*; Ahrens, T. J., Ed.; American Geophysical Union: Washington, DC, 1995.
(64) Misawa, M.; Price, D. L.; Suzuki, K. *J. Non-Cryst. Solids* **1980**, *37*, 85.
(65) Poulsen, H. F.; Neuefeind, J.; Neumann, H. B.; Schneider, J. R.; Zeidler, M. D. *J. Non-Cryst. Solids* **1995**, *188*, 63.
(66) Clark, T. M.; Grandinetti, P. J.; Florian, P.; Stebbins, J. F. *Phys. Rev. B* **2004**, *70*, 064202.

(67) Appen, A. A. *Chemistry of Glass*; Khimiya: Leningrad, 1970 (in Russian).
(68) Gan Fuxi *Sci. Sin.* **1974**, *17*, 533.
(69) Demkina, L. I. *Izd. Chimia* **1976**, *23*, 123.
(70) Priven, A. I. *Glass Technol.* **2004**, *45*, 244.
(71) Sierka, M.; Sauer, J. *Faraday Discuss.* **1997**, *106*, 41.
(72) Thong N. G. O.; Schwarzenbach D. *Acta Crystallogr., Sect. A* **1979**, *35*, 658.
(73) Ecolivet, C.; Poignant, H. *Phys. Status Solidi* **1981**, *63*, K107.
(74) Wang, H.; Xu, B.; Liu, X.; Han, J.; Shan, S.; Li, H. *J. Cryst. Growth* **1986**, *79*, 227.
(75) Dick, B. G.; Overhauser, A. W. *Phys. Rev.* **1958**, *112*, 90.
(76) Sanders, M. J.; Leslie, M. J.; Catlow, C. R. A. *J. Chem. Soc., Chem. Commun.* **1984**, 1271.
(77) Pascale, F.; Catti, M.; Damin, A.; Orlando, R.; Saunders: V. R.; Dovesi, R. *J. Phys. Chem B* **2005**, *109*, 18522.
(78) Orlando, R.; Torres, F. J.; Pascale, F.; Ugliengo, P.; Zicovich-Wilson, C.; Dovesi, R. *J. Phys. Chem. B* **2006**, *110*, 692.